IMPROVING PERFORMANCE OF POLYMER FIBER REINFORCED SANDWICH X-JOINTS IN NAVAL VESSELS – PART II: DAMAGE TOLERANCE

Christian Lundsgaard-Larsen*, Christian Berggreen*, Kasper Karlsen*, Claus Jenstrup* and Brian Hayman**
***Department of Mechanical Engineering, Technical University of Denmark**
****Det Norske Veritas and University of Oslo, Norway**

Keywords: *Sandwich, X-joint, debond, fiber bridging, cohesive laws*

Abstract

This study deals with damage tolerance of sandwich X-joints with embedded debond damages between face and core. The study is conducted both through modeling and full-scale tests. Mixed mode cohesive laws from the opening of sandwich interfaces are determined experimentally from a DCB specimen loaded by moments, and the results are utilized in a cohesive zone model of a tested sandwich structure. Results of the crack propagation from experiments and simulation show fair agreement. Design aspects regarding the influence of debond size and core inserts on the residual strength are discussed.

1 Introduction

In the last decade the use of sandwich structures has increased tremendously in applications where low weight is of importance e.g. certain types of naval ship structures, where the sandwich panels are often built up with fiber reinforced faces and foam core. In sandwich structures there is often a need to assemble panels in out-of-plane joints, designated T-joints or X-joints, where one or two panels are attached perpendicularly to the faces of another panel which extends continuously through the joint. Loading of the attached panels entails out-of-plane loads acting on the faces of the continuous panel. In the compression case this can lead to indentation and crushing of the core, whereas the tension case can lead to debonding and face pull-off. Furthermore, crushing of the core can lead to debonded areas which can act as a starting crack. When loaded in tension these may propagate through a large part of the structure. Thus, a joint that has been damaged in compression may fail under tension loads significantly smaller than for an intact joint. Crack propagation in glass fiber reinforced faces entails large scale fiber bridging, which increases the size of the process zone beyond a point where linear elastic fracture mechanics (LEFM) is applicable. Therefore a cohesive zone model is used to simulate the process zone mechanisms such as fiber bridging, plasticity and friction, separately or in combination.

Besides analyzing the strength of X-joints loaded in tension, the aim of this study is to establish a method for conducting simulations, where the face-core interface fracture properties are initially measured from a unique test method, and later applied in a finite element model at a structural level to predict crack propagation.

The paper is organized as follows:

- A recently developed test method for measuring cohesive laws for the interface of sandwich specimens is reviewed and results presented.
- An experiment with a sandwich beam loaded by traction forces perpendicular to the face is described.
- A finite element model utilizing the measured cohesive law is used to predict crack propagation for the conducted experiment.
- Experimental and numerical results are presented and compared.

2 Determining cohesive laws experimentally

The following section describes the test method used for determining the traction separation behavior of a sandwich interface.

2.1 Test method

The test method is based on a Double Cantilever Beam specimen loaded by Uneven Bending Moments (DCB-UBM), see Fig. 1. For a thorough description of the test rig, see [1]. The test is conducted under displacement control in a tensile test machine, and the moment ratio is kept constant throughout one test. Stable crack growth is accommodated, since the J integral is independent of crack length for a DCB specimen loaded by pure moments [2].

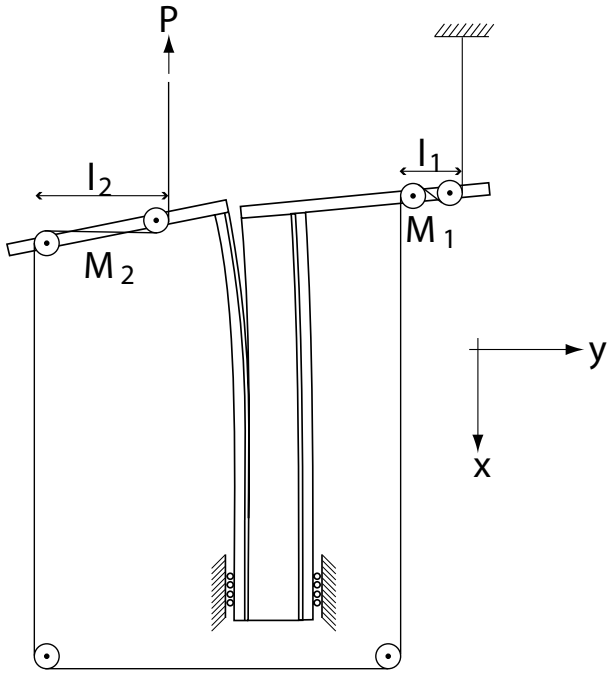

Fig. 1. Schematic of a DCB sandwich specimen loaded by moments.

The moments are obtained from forces applied by a roller-wire system to bars attached to the top of the specimen. The load is applied by a single wire, thereby ensuring that the four vertical forces acting on the rollers are equal in size. The moments acting on the left and right beams are determined from the force in the wire and the distance between rollers. It is seen that

$$M_1 = pl_1 \qquad M_2 = pl_2 \tag{1}$$

where M_1 and M_2 are moments acting on the right and left beam respectively, positive in counter-clockwise direction.

The ratio between M_1 and M_2 is changed by adjusting the relative distance between rollers. Furthermore the direction of the moments can be reversed by changing the mounting direction of the wire. If moments with opposite signs are applied e.g. $M_1/M_2 = -1$, crack opening in the normal direction is dominating (Mode I). If moments with the same sign are applied the crack opening in tangential direction is more dominating (Mode II). It is possible to vary the loading and hereby the normal/tangential crack opening ratio δ_n^*/δ_t^* to almost any preferred value. The test is conducted for four different moment ratios and each repeated three times resulting in a total of 12 tested specimens. More details on the test method and analysis of the specimen are found in [3].

2.2 Fracture toughness and derived cohesive laws

The following describes shortly the principle behind extracting cohesive laws using a J integral approach. By relating the J integral to the normal and tangential opening of the initial crack tip, δ_n^* and δ_t^*, a cohesive law can be determined. The relation between J integral and cohesive stresses is found by applying the J integral locally around the crack faces [2,4].

$$J_R = \int_0^{\delta_n^*} \sigma_n(\delta_n, \delta_t) d\delta_n + \int_0^{\delta_t^*} \sigma_t(\delta_n, \delta_t) d\delta_t \tag{2}$$

where σ_n and σ_t denote the normal and shear stresses, respectively, in the cohesive zone. As indicated by Eq. 2 the cohesive stresses are assumed to depend only on the local openings, δ_n^* and δ_t^*, and not on the opening path. By differentiating Eq. 2 with respect to δ_n^* and δ_t^*

$$\frac{\partial J_R(\delta_n^*, \delta_t^*)}{\delta_n^*} = \sigma_n(\delta_n^*, \delta_t^*) \qquad \frac{\partial J_R(\delta_n^*, \delta_t^*)}{\delta_t^*} = \sigma_t(\delta_n^*, \delta_t^*) \tag{3}$$

where $\sigma_n(\delta_n^*, \delta_t^*)$ and $\sigma_t(\delta_n^*, \delta_t^*)$ are stresses between the crack faces as function of normal and tangential opening of the pre-crack tip. From Eq. 3

the cohesive law can be obtained directly from J_R and measured values of δ_n^* and δ_t^*.

The opening displacements δ_n^* and δ_t^* are found from optical measurements and the J value is calculated from the applied moments, specimen geometry and elastic properties (see [3] for further details). The output from each experiment is J as a function of δ_n^* and δ_t^*, and a fracture toughness surface plot is created using linear interpolation between the experimental data sets. The generated surface is seen in Fig. 2.

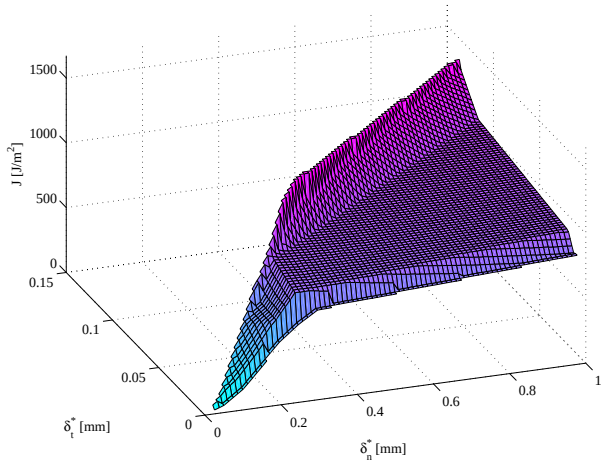

Fig. 2. Fracture toughness *J* as function of pre-crack tip opening components δ_n^* and δ_t^*.

Consider the J value for increasing δ_n^* in Fig. 2. It is found that the fracture toughness increases first rapidly for small openings, whereas at some point the surface changes slope, and from here on the fracture toughness increases slowly. The physical interpretation of the fracture toughness history is that the rapid increase is caused by elastic deformation and cracking of the material near the crack tip, whereas the slow increase after the surface changes slope is a result of the fiber bridging mechanisms when the material separates.

The derived cohesive laws are found by partial differentiation of the fracture toughness surface using Eq. 3, and an example of derived cohesive laws along a path given by $\delta_n^* = 20\delta_t^*$ is seen in Fig. 3

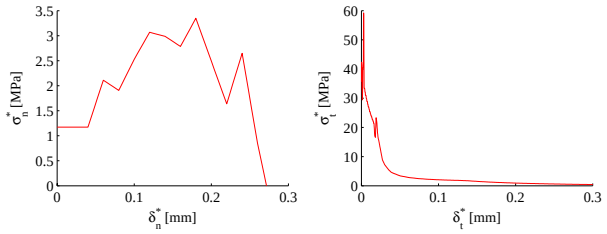

Fig. 3. Derived cohesive laws from the surface plot in Fig. 2 found along a path $\delta_n^* = 20\delta_t^*$

The maximum normal and tangential stresses reach approx. 3 and 60 MPa respectively, and the found shape of the cohesive laws for normal and tangential opening directions are very different. The maximum fracture toughness for the chosen path of $\delta_n^* = 20\delta_t^*$ is found from the fracture toughness surface plot in Fig. 2 to be approx. 900 J/m^2, which corresponds to the sum of the areas below the curves, seen in Fig. 3.

The cohesive laws for other paths found for the surface in Fig. 2 are qualitatively similar to the shapes seen in Fig. 3, however the maximum normal stress varies between 3 and 5 MPa and the maximum tangential stress varies between 8 and 60 MPa. The maximum stresses are calculated for very small displacement, and are therefore subjected to some uncertainty (this goes especially for stresses in the tangential direction).

Some approximations are necessary when implementing the measured cohesive laws in the commercial FE-code ABAQUS, which is described in section 4.2..

3 Tear-off experiment

This chapter describes the experiment of loading the face of a sandwich beam in out-of-plane tension. The experiment represents the fracture scenario as a critical tensile force is applied to the through-going panel of an X-joint.

3.1 Test-rig and specimen specifics

The following describes the test-rig and specimens used for conducting a sandwich face tear-off test, where the face of a sandwich beam is subjected to a load perpendicular to the face. The sandwich specimen is mounted in the same test-rig as used in part I of this paper [5], and again the specimen is loaded by an Instron 8502 servo-hydraulic test machine , see Fig. 4

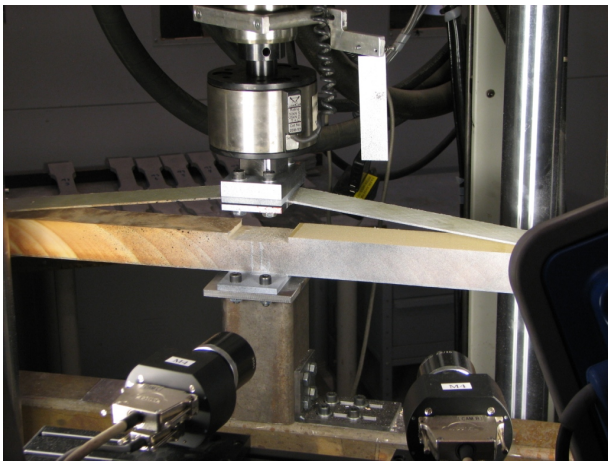

Fig. 4. Loaded specimen in tensile test machine. Notice cameras and speckled pattern on specimen used for measuring displacement of specimen surface.

The middle of the bottom face is fixed to the test-rig, and the middle of the top face is fixed to the cross-head, see Fig. 4. The sandwich specimen has wooden inserts at the ends which are clamped to the test-rig. A Teflon film is inserted between the face and core along half the specimen length, so that the crack will only propagate to one side and hence only one fracture incidence will occur in the measurements. The reason for not only performing the experiment on the specimen half where crack propagation occurs is that during the experiment the tension in the face becomes very large, and this generates side forces on the cross head, which might damage the machine. The beam half with the Teflon film incorporated provides some symmetry, and takes up some of the side forces.

The specimen is loaded as seen in Fig. 4 by moving the cross-head upwards with a rate of 2 mm/min, ensuring that all inertia effects are negligible. Each specimen is loaded 30-40 mm before the crack is fully propagated. The displacement field of the specimen surface is recorded using a commercial optical system (ARAMIS 4M), where each point on a selected part of the specimen surface is accurately followed by the system software. A speckled pattern is applied to the specimen surface using spray paint and a thin layer of first white and then black paint is applied to ensure a high contrast speckled pattern. A picture rate of 1 frame per 4 seconds is chosen appropriate to be able to follow the deformation field (and hereby the crack length), without needing to process an unnecessarily large amount of data. The software can recognize each point on the speckled pattern and is able to calculate the displacement field by comparing with the frame of the initial un-deformed specimen. The force is measured using a 50 kN load cell with an accuracy of 0.005 % of the load cell's capacity. The dimensions of the test specimen are given in Fig. 5.

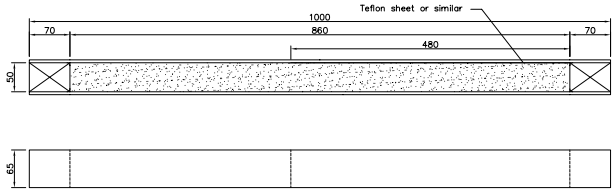

Fig. 5. geometry of damage tolerance specimen, dimensions in mm.

The sandwich specimen is constructed using four DBLT 850 quadri-axial mats each with density of approximately 850 g/m^2, which gives an approximate face thickness of 2.9 mm. The sandwich core is of Divinycell H200, 50 mm thick and with a density of 200 g/m^2. Material properties are found from tests and are given in [5].

3.2 Observations during test

As mentioned previously, the load is applied displacement controlled by a rate of 2 mm/min until the crack is propagated from the center to the end support. During this time the crack propagates slowly, with an increasing amount of fiber bridging, which implies that the size of the process zone is large, and needs to be accounted for (which is not the case in LEFM). The specimen with a fully propagated crack is seen in Fig. 6.

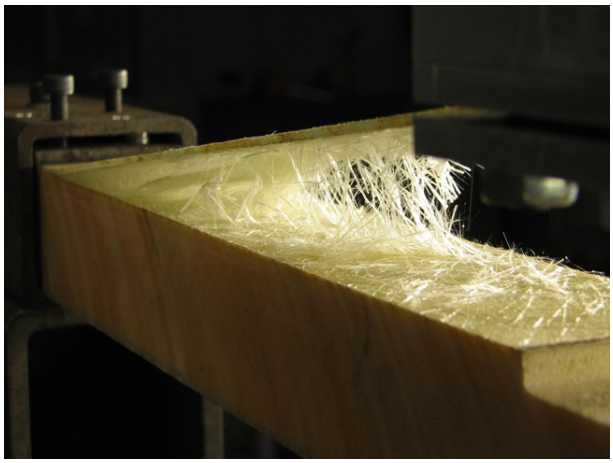

Fig. 6. Bridging fibers are connecting the crack faces of the specimen.

The specimen is loaded by moving the cross-head upward (in the y-direction). The specimen is

not perfectly symmetrical, since Teflon film is inserted along half the specimen during production, to prevent bonding between face and core for this region in order to avoid mixed results when having two cracks propagating. As the crack propagates toward the end support, the specimen becomes gradually symmetrical, since the crack is then extended equally in both directions. The effect of the asymmetry on the cross head displacement in the x-direction is investigated using the digital optical measurement system, ARAMIS. The displacement in the horizontal direction δ_x is plotted as a function of displacement in the vertical direction δ_y in Fig. 7.

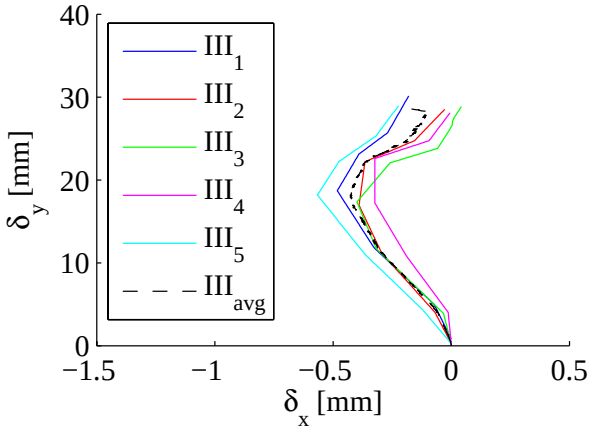

Fig. 7. Crosshead displacement in the vertical (loading direction) and horizontal directions.

From Fig. 7 it is found that the horizontal displacement reaches a maximum of approx. 0.5 mm at a vertical displacement of 20 mm. This measurement is used in the finite element model described in chapter 4.

3.3 Collecting data

The following data are collected from the experiments and used for comparison with the finite element model.

- **Time**; used to synchronize other data
- **Lift**; equal to the test machine piston displacement, which is proportional to the time with a displacement rate of 2 mm/min.
- **Lift force**; data given as output from the load cell
- **Crack length**; the crack length is found by tracking the opening between the core and face at different locations along the interface.

The crack length is estimated from the opening of 12-14 points along the interface. As the opening between face and core at one location can no longer be interpreted as elastic, the crack tip is assumed to have passed this position. Since the crack propagates slowly, it is assumed that the crack tip position can be interpolated between the given points. The collected data is presented in the Analysis and results chapter.

4 Finite element model

This chapter describes the finite element model used for simulating the previously mentioned experiment.

4.1 General assumptions

A 2D finite element model is created in the commercial FE-code ABAQUS version 6.6 and the explicit solver is used. Due to symmetry only half the specimen is modeled. A schematic illustration of the model is given in Fig. 8.

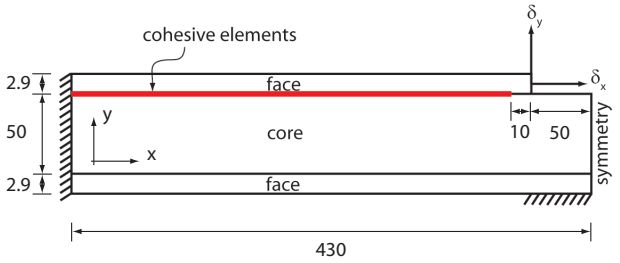

Fig. 8. Schematic drawing of the finite element model indicating boundary conditions, cohesive section and loading points.

Due to symmetry only half the specimen is modeled. The model consists of two faces and a core, where the top face and the core are connected through zero-thickness cohesive elements which represent the traction-separation behavior in the interface, see Fig. 8. The left edge of the sandwich beam is fixed, and the right edge is exposed to symmetry conditions. A length of 50 mm of the bottom right edge is fixed, since this part is clamped to the test rig in the experiments. The dimensions of the model are shown in Fig. 8 and are similar to those of the real specimen.

The finite element model is meshed uniformly with 4 node bilinear rectangular elements each with 8 degrees of freedom. The element size is approximately 0.5 mm, which corresponds to 6 elements through the thickness direction of the face. The sandwich specimen is loaded in displacement

control as indicated in Fig. 8, so that the edge of the face is displaced. As mentioned previously the displacements in the vertical and horizontal directions are measured with the optical system during the experiments, see Fig. 7. The displacement applied to the face edge nodes in the finite element model follows an approximation of the measured displacements in x- and y-direction respectively, which is illustrated in Fig. 9. This approach is similar to a study described in [7].

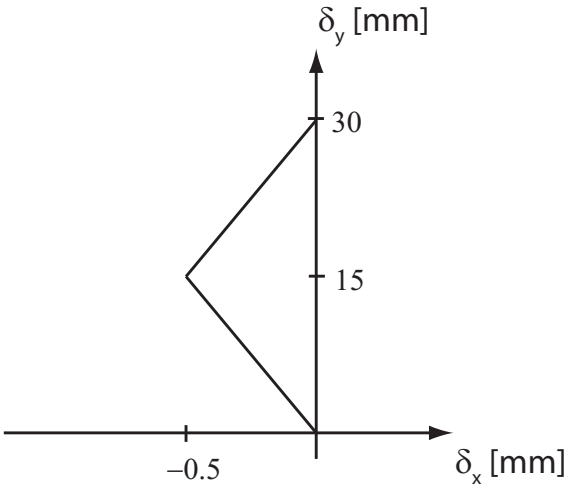

Fig. 9. Displacement curve applied to the finite element model.

The loading rate is chosen sufficiently low, so that inertia effects are negligible (kinetic energy is below 1% of the total energy in the system). In the experiment the face edge is clamped to the cross-head of the machine, so the loaded edge in the numerical model, see Fig 8, is restricted from rotating. Convergence regarding element size and time increment size is found by varying them both.

4.2 Cohesive laws and damage evolution

The following describes the implementation of the measured cohesive law in ABAQUS. The constitutive behavior of the cohesive elements is described using a traction-separation (cohesive) law, hereby transferring traction forces between the face and the core as they separate. The measured cohesive law is approximated with a triangular shaped cohesive law, which is uniquely determined in ABAQUS by three different parameters:

- Slope of the initial linear branch
- The maximum stress (damage initiation point)
- Area below the curve.

It is believed that these three parameters are the most important regarding the outcome from the model, and that the detailed shape of the cohesive law therefore plays only a smaller role. The three parameters are given for the normal stress during pure normal loading (mode I) and for tangential stress during pure tangential loading (mode II). For any intermediate loading (mixed mode), ABAQUS interpolates between the given cohesive laws. The different parameters are indicated on Fig. 10.

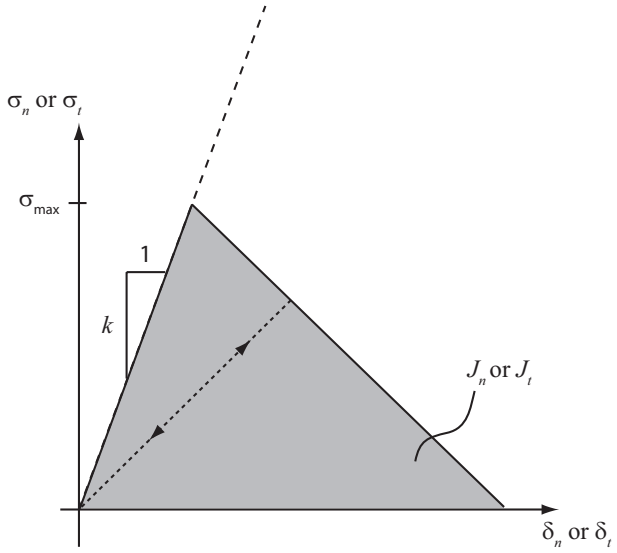

Fig. 10. Schematic shape of assumed cohesive law

The parameters for the implemented cohesive laws are given in Table 1.

Table 1. Parameters defining the constitutive behavior for the implemented cohesive elements. k is slope of initial linear branch, $\sigma_{\max}$ is the stress at damage initiation and J is the fracture energy.

	Pure normal	Pure tangential
k [Pa]	$5{\cdot}10^{10}$	$5{\cdot}10^{11}$
$\sigma_{\max}$ [Pa]	$3{\cdot}10^{6}$	$50{\cdot}10^{6}$
J [J/m^2]	800	2000

The slope of the initial linear branch, k, is to be sufficiently large so that no significant artificial elasticity will be added to the intact part of the structure. The chosen stiffness of $5{\cdot}10^{10}$ Pa given in Table 1 corresponds to 200 times the E-modulus of the core material, see [5]. The point of damage initiation is determined by the maximum stress given by the criterion

$$\max\left\{\frac{\langle\sigma_n\rangle}{\sigma_n^o},\frac{\sigma_t}{\sigma_t^o}\right\}=1 \qquad (4)$$

where the symbol $\langle\ \rangle$ represents the Macaulay bracket, indicating that a compressive normal stress

will not lead to damage initiation. The subscript *n* indicates stress in pure normal direction and *t* in pure tangential. ABAQUS adjusts the decreasing part of the cohesive law, so that the area below the curve is equal to the fracture energy specified from the failure criterion.

The mode mixity measure is given in form of tractions as

$$\phi = \frac{2}{\pi}\arctan\left(\frac{\sigma_t}{\langle\sigma_n\rangle}\right) \quad (5)$$

so that for pure normal stress the mode mixity ratio $\phi = 0$, and for a pure tangential stress $\phi = 1$. The mode mixity measure controls the interpolation between the parameters given for pure mode I and II in Table 1.

5 Analysis and results

In this chapter results from the experiments and finite element model are described, discussed and compared.

5.1 Length of process zone

The process zone length is defined as the distance between the point of damage initiation and point of complete damage (cohesive elements are stress-free), see Fig 10. To have an accurate representation of the cohesive zone, the size of the process zone should span several cohesive elements [6]. A stress plot of the process zone and the area around it is shown in Fig. 11.

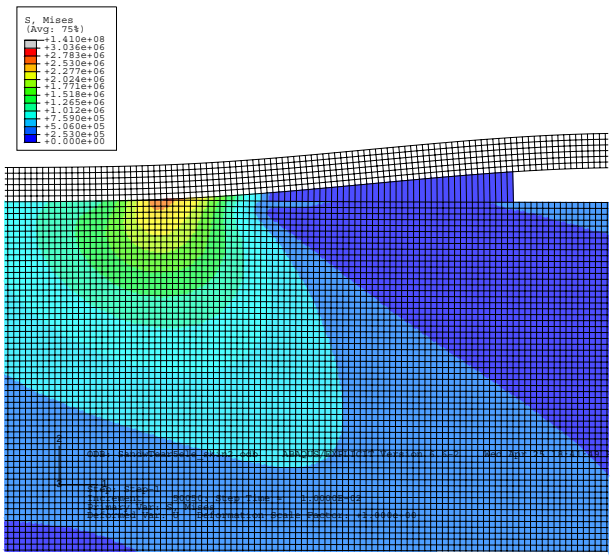

Fig. 11. The von Mises stress near the crack tip. The element length is approx. 0.5 mm.

From Fig. 11 it is found that the number of cohesive elements that are in a state between damage initiation and complete damage is approximately 20, which corresponds to a process zone length of 10 mm. This is assumed to be sufficient for a good representation of the cohesive zone.

5.1 Results from experiments and FE

The following describes and compares the results obtained from the experiments and the finite element simulation. Initially the experimental and numerical results are commented on independently, and later results are compared.

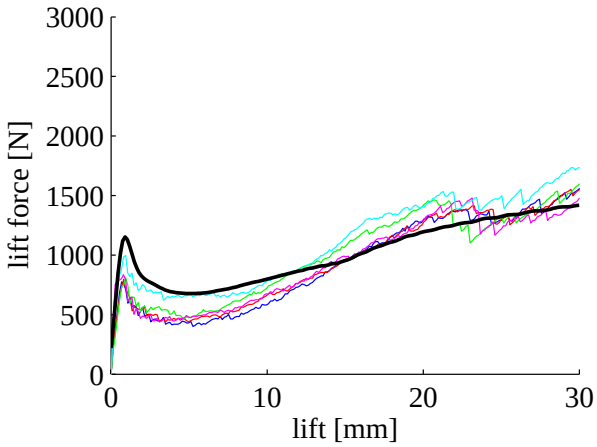

Fig. 12. Lift force as function of lift displacement. Thin colored lines are experiments and thick black line is simulation.

The force-displacement history from the experiments and simulation consist of several phases as indicated by Fig. 12. Initially the relation between force and displacement is close to linear, which corresponds to opening of the pre-crack. As the conditions for crack propagation are met (stress in the cohesive element behind the crack tip exceeds σ_{max}), the crack propagates and the lift force drops to a local minimum of approx. 60% of the peak stress as the lift reaches 5 mm. As the crack propagates further with increasing lift displacement the mode mixity conditions near the crack tip changes toward more mode II. Further large scale fiber bridging develops as shown in Fig. 6, which causes the fracture toughness to increase, and the lift force to increase as well. Results are qualitatively similar to the experimental obtained results described in [8].

Generally it is found that the numerical estimation is in fair agreement with the experiments. The numerical results are somewhat un-conservative since they show higher strength than the experimental results, and the peak strength is 25-50% bigger for the simulation compared to the individual experiments. The difference decreases however as the crack propagates.

As mentioned previously the crack length from the experiments is estimated from the opening displacement of points along the interface. The same is conducted for the finite element model, and the crack length as function of lift displacement is plotted in Fig. 13.

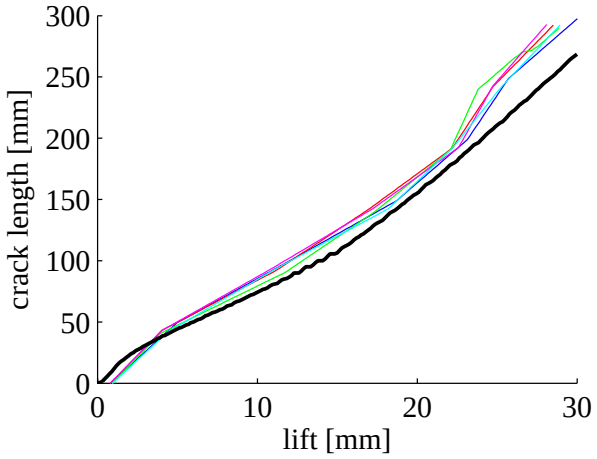

Fig. 13. Estimated crack length as function of lift displacement. Thin lines are experiments, thick is simulation.

The crack propagation length as function of lift displacement is found to be a little smaller for the simulation compared to the experiments, especially towards the end of the experiment, where the mode mix changes toward more mode II. This could indicate that the assumed mode mix measure, which controls the fracture energy in the cohesive zone, is less accurate towards more mode II conditions. The deviations are however found to be within the acceptable limit, considering the sources of error connected with measuring the crack length for the experiments.

The lift force as function of crack length for the experiments and simulation is plotted on Fig. 14.

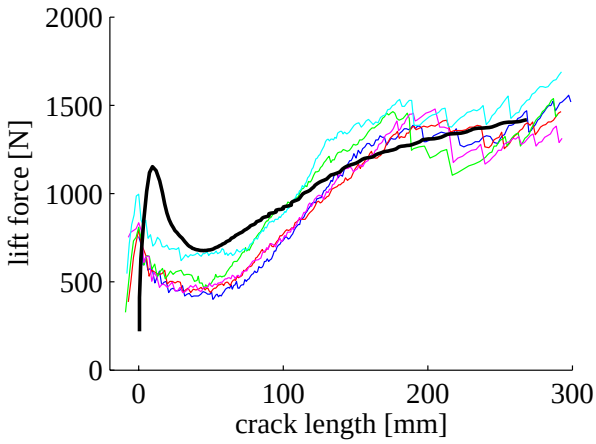

Fig 14. Lift force as function of crack length.

As seen in Fig. 14 the lift force reaches a local maximum just before the crack starts propagating, which relates well with the plot in Fig. 12. Regarding the comparison between experimental and numerical results the observations are similar to the ones described previously.

The plot shown in Fig. 14 is useable when considering the residual strength of joints with a debond present. The plot gives the lift force (design load) as function of crack length (debond size). This is described in further detail in the following chapter.

6 Design guidance

As mentioned in part I of this paper [5], the strength of the X-joint can be improved by replacing a block of the core material in the through going panel of the joint with a stronger material. It is likely that the core insert will strengthen the joint in both compression and tension, where compression is investigated in [5] and tension is considered in this study. If a demand for damage tolerance exists, and the joint should be able to withstand design loads with debonds present, the results from this study are useful for determining the necessary core insert length as function of tensile design load. For the design case it is assumed that a block of H200 core material is used as an insert in a weaker core material to strengthen the structure. The core insert length is computed under the assumption that the panel attached perpendicularly to the through-going panel of the X-joint is 80 mm thick (same as the clamp used for the experiments). The influence of the initial debond size on the loading history is shown in schematic form in Fig. 15.

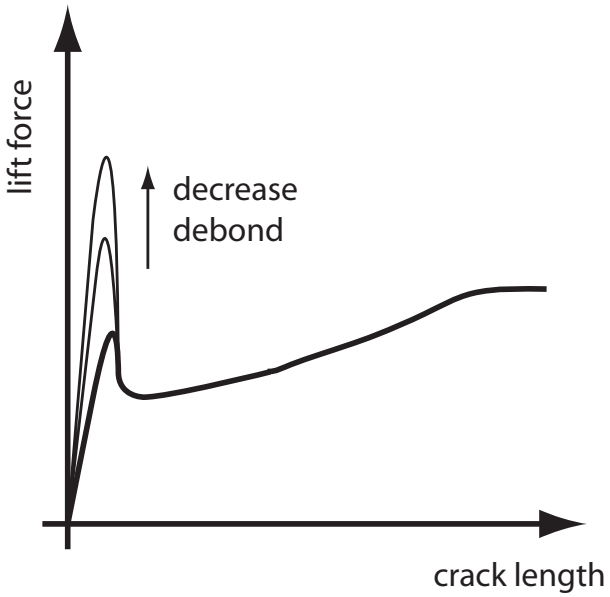

Fig 15. Schematic relation between lift force and crack propagation length for various initial debond sizes.

As indicated by Fig. 15, the maximum force the joint can resist depends on the initial debond, such that the strength of the panel increases with decreasing debond size and the highest strength is reached for an intact joint. The strength of the joint after the crack has propagated is given as the non-linear part in Fig. 15. The maximum load the damaged joint can resist can be found as a function of crack length, from the results shown in Fig. 14. The insert length needs to be sufficiently large so that the crack will not propagate into areas without a core insert. Results are normalized with respect to the depth, and the minimum insert length as function of applied load is shown in Fig. 16.

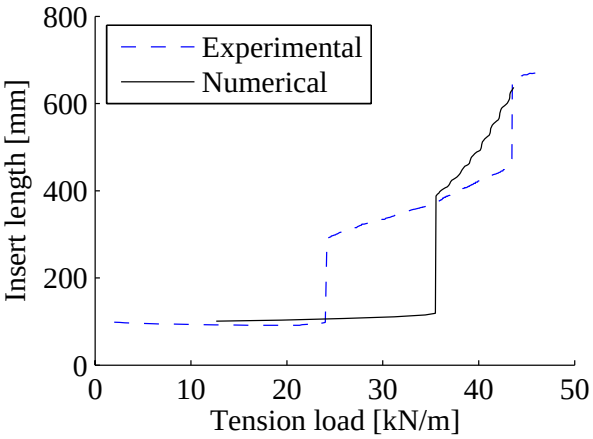

Fig. 16. Minimum core insert length as function of design tension load. Dotted line is average experimental data and solid line represents the simulation.

When considering the experimental data, a design tension load of e.g. 40 kN would require a core insert of approx. 400 mm. A similar plot is given for the compression case in [5].

7 Conclusion and future work

7.1 Conclusion

This study deals with predicting and measuring the residual strength of a sandwich panel with an initial debond damage. This is conducted using a cohesive zone model and full scale tests of a sandwich beam loaded by tractions perpendicular to the face. Mixed mode cohesive laws are initially determined experimentally from a DCB specimen loaded with moments, and the results are utilized in a cohesive zone finite element model. Results from experiments and simulation show fair agreement, and indicate that the method is usable for the given damage scenario. Design aspects regarding the influence of debond size and core inserts on the residual strength are discussed.

7.2 Future work

The experimentally found cohesive law is approximated with a triangular shape, and ABAQUS interpolates between a state of pure normal opening with pure normal stress (mode I) and pure tangential opening with pure shear stress (mode II), see section 4.2. Since the cohesive law is given as the normal and shear stress for any intermediate mixed mode conditions (not interpolated between pure mode I and II), this is a radical approximation, which needs further attention in the future.

The study is conducted under the assumption of similar condition through the thickness direction (2D), which is not likely in a real structure. Analysis regarding different load distributions or shapes of the initial debond in the through thickness direction requires the use of a 3D model, which could be developed in future work.

8 Acknowledgements

This work has been performed within the context of the Network of Excellence on Marine

Structures (MARSTRUCT) partially funded by the European Union through the Growth Programme under contract TNE3-CT-2003-506141. The provision of test specimens by Kockums AB (Karlskronavarvet) is highly appreciated.

References

[1] Sørensen, B.F., Jørgensen, K, Jacobsen, T.K., Østergaard, R.C., "DCB-specimen loaded with uneven bending moments". *International Journal of Fracture*, Vol. 141, No. 1-2, pp 163-176, 2006.

[2] Suo, Z., Bao, G. and Fan, B. "Delamination R-curve phenomena due to damage." *Journal of the Mechanics and Physics of Solids*. Vol 40, pp 1–16. 1992.

[3] Lundsgaard-Larsen, C., Sørensen, B.F., Berggreen, C. and Østergaard, R.C., "A modified DCB sandwich specimen for measuring mixed mode cohesive laws". *Engineering Fracture Mechanics*, submitted, 2007.

[4] Sørensen, B.F. and Kirkegaard, P. "Determination of mixed mode cohesive laws". *Engineering Fracture Mechanics,* Col. 73, No 17, pp 2642-2661, 2006

[5] Berggreen, C., Lundsgaard-Larsen, C., Karlsen, K., Jenstrup, C. and Hayman, B., "Improving performance of polymer fiber reinforced sandwich X-joints in naval vessels – Part I: Design Aspects". *16th International Conference on Composite Materials*, Kyoto, Japan, 2007.

[6] Yang, Q., and Cox, B.N., "Cohesive models for damage evolution in laminated composites". *International Journal of Fracture*, Vol 133, No 2, pp 107-137, 2005

[7] Berggreen, C., Jensen, C. and Hayman, B., "Buckling strength of square composite plates with geometrical imperfections – preliminary results". *MARSTRUCT International Conference on Advancements in Marine Structures*, Glasgow, UK, 2007.

[8] Berggreen, C., Simonsen, B.C. and Borum, K.K., "Experimental and numerical study of interface crack propagation in foam-cored sandwich beams". *Journal of Composite materials*, Vol 41, No 4, pp 493-520, 2007